nature communications

Article

https://doi.org/10.1038/s41467-025-55990-z

Room-temperature phosphorescent transparent wood

Received: 10 January 2024

Accepted: 7 January 2025

Published online: 20 January 2025

Check for updates

Xixi Piao, Tengyue Wang, Xuefeng Chen, Guangming Wang, Xiangxiang Zhai & Kaka Zhang

Transparent wood with high transmittance and versatility has attracted great attention as an energy-saving building material. Many studies have focused on luminescent transparent wood, while the research on organic afterglow transparent wood is an interesting combination. Here, we use luminescent difluoroboron β-diketonate (BF_2bdk) compounds, methyl methacrylate (MMA), delignified wood, and initiators to prepare room-temperature phosphorescent transparent wood by thermal initiation polymerization. The resultant PMMA has been found to interact with BF_2bdk via dipole-dipole interactions and consequently enhance the intersystem crossing of BF_2bdk excited states. The transparent wood matrix can provide a rigid environment for BF_2bdk triplets and serve as oxygen barrier to suppress non-radiative decay and oxygen quenching. The prepared afterglow material has the characteristics of diverse composition, long afterglow emission lifetimes, and high photoluminescence quantum yield. This afterglow transparent wood also demonstrates potential application value in areas such as high mechanical strength, good hydrophobicity, and high cost-effectiveness.

Developing green materials with certain advantages and functional characteristics using renewable resources is beneficial for achieving sustainable development goals. Wood as a kind of green material, is a widely used porous material with characteristics such as low density, high modulus, high strength, high toughness, and low thermal conductivity[1–5]. Due to its distinctive microstructure and composition, transparent wood prepared from wood exhibits good optical properties, high strength-to-weight ratio, and hierarchical structure, making it a promising biomaterial-derived material[6]. It also possesses excellent properties such as high transparency and good mechanical strength[7,8], making it applicable in various fields such as optoelectronic devices[9–12], energy-efficient buildings[13,14], thermal energy storage[15–17], solar cells[18–20], and UV absorption[21–23].

Room-temperature phosphorescence (RTP) and organic long persistent luminescence (OLPL) materials are a class of luminescent materials that have longer emission lifetimes than fluorescent materials[24–26]. Conventionally, RTP materials with phosphorescence lifetime (τ_P) longer than 100 ms are considered as room-temperature afterglow materials[27–29], because the RTP property of such materials can be readily recorded by inexpensive equipment and even distinguished by cameras and human eyes; these luminescent behaviors enable RTP afterglow materials' broad applications in areas such as oxygen analysis, mapping, anti-counterfeiting, data encryption, background-free bioimaging, and time-gated optical sensing[30–36].

For transparent wood, the involvement of RTP afterglow property would endow the materials with display, esthetics, personalized customization, and science popularization functions. For RTP materials, the transparent wood matrices mean that excitation light can easily enter to excite the luminescent molecules inside, and then penetrate out to show bright afterglow property. Besides, the introduction of wood into RTP material system can reduce the amount of synthetic polymer used. In addition, the involvement of wood component would provide excellent mechanical property for RTP material system[6]. Moreover, because of the presence of rich hydrogen bonding and

State Key Laboratory of Organometallic Chemistry and Shanghai Hongkong Joint Laboratory in Chemical Synthesis, Shanghai Institute of Organic Chemistry, University of Chinese Academy of Sciences, Chinese Academy of Sciences, 345 Lingling Road, Shanghai 200032, People's Republic of China.
e-mail: zhangkaka@sioc.ac.cn

relatively high crystallinity of cellulose fibrils in wood, the wood component can suppress oxygen diffusion to protect organic triplet excited states in RTP material system. Therefore, the combination of transparent wood and RTP afterglow would exhibit broad prospects. There are reported stuides on the versatile fabrication of wood-based RTP materials[37–40], but not on RTP transparent wood. It has been reported that RTP transparent wood showed RTP duration around 200 ms in the literature (Supplementary Discussion)[41]. It is known that materials' RTP duration can reach about 5–10 folds of their τ_P[32,34,42,43], so RTP duration around 200 ms would refer to a τ_P of around several tens of milliseconds. To our knowledge, there have been no reports on the preparation of transparent wood as room-temperature organic afterglow materials with $\tau_P > 100$ ms, for example, τ_P of 1 s and even 10 s.

In actuality, it is not only difficult to achieve transparent wood of long τ_P, but it is also challenging in conventional organic systems to obtain high-performance RTP and OLPL materials with high quantum efficiency or long emission lifetime or both in environmental conditions due to the spin-forbidden nature of intersystem crossing and afterglow quenching in organic systems[44–50]. To address this issue, groundbreaking research has demonstrated that design strategies based on heavy atom effects, n-π* transitions, molecular crystallization, control of aggregation, and supramolecular assembly can enhance RTP and organic persistent luminescence efficiency[31–35]. Additionally, our research group has discovered various organic afterglow materials with excellent photophysical properties through dopant-matrix design strategies[50–57]. In donor-acceptor systems, appropriate combinations of organic molecules can produce OLPL lasting for several hours through photo-induced charge separation and subsequent delayed charge recombination[58,59]. Recent studies have shown that these RTP and OLPL systems can maintain afterglow characteristics when exposed to environmental conditions or even dispersed in an aqueous medium[60–65]. The dopant-matrix design strategies allow for flexible selection of luminescent dopants and organic matrices to construct RTP and persistent luminescent materials with different structures and compositions[66–70]. For example, specific polymer matrices provide a rigid environment that inhibits nonradiative decay of the triplet excited state (k_{nr}), thus constructing organic RTP and persistent luminescent materials[66,71,72]. Poly(methyl methacrylate) (PMMA), a low-cost petroleum-based polymer, is widely used as polymer matrix due to its high transparency, low density, low toxicity, excellent durability, and controllability. Various PMMA-based RTP materials with anti-counterfeiting and data encryption functions have been reported[66,71–76]. The dopant-matrix design strategy allows the polymer component to control the excited state property of the luminescent component, resulting in polymer-based organic RTP and afterglow materials with excellent mechanical properties[77,78]. Solution casting is the most commonly used technique for preparing polymer-based RTP materials[77–80]. However, it requires a large amount of solvent, and the evaporation process is slow, making the preparation process time-consuming. On the other hand, melt casting technology is frequently applied in polymer processing as it avoids the use of solvents[81], but it requires high temperatures and also leads to energy waste. When preparing polymer-based RTP materials by melt casting, some of the luminescent dopants may undergo decomposition at relatively high temperatures. Solvent-free and time-saving methods under mild condition via photopolymerization have also been developed for the preparation of polymer-based RTP materials[82].

On the basis of the above advancements in the fabrication strategies of RTP and organic afterglow materials, particularly those in polymer-based RTP systems, here we design high-performance RTP transparent wood by simultaneously considering the requirements of material fabrication from both aspects of efficient and long-lived RTP and robust transparent wood. In the process of preparing transparent wood, the impregnated resin requires itself to be transparent without visible light absorption, have a refractive index similar to that of wood fibers, and have good compatibility with mother fibers[1–23,73]. Therefore, PMMA is highly regarded as a suitable resin for fabricating transparent wood. We conceive that if the luminescent dopant, monomer, macromolecular matrix framework, and certain initiators can be converted into polymers at an appropriate temperature, the molecular motion of the dispersed luminescent dopants in the formed polymer can be greatly suppressed. This would establish a solvent-free method for preparing polymer-based RTP materials. In addition, the design of luminescent dopants is essential for the preparation of RTP materials with long afterglow duration and high afterglow efficiency. Luminescent difluoroboron β-diketonate (BF_2bdk) compounds have been proven to possess interesting optical properties, including large molar absorption coefficients and high photoluminescence quantum yields (PLQY) in both solution and solid states. They also exhibit a wide range of tunable emission spectra with intramolecular charge transfer (ICT) characteristics. BF_2bdk molecules have become excellent building blocks in dopant-matrix systems for designing high-performance and functional afterglow materials. Therefore, in this study, we prepared a room-temperature phosphorescent multifunctional transparent wood based on PMMA/wood. The collaboration of wood and PMMA leads to the enhancement of afterglow property. Besides its sustainable nature, the wood component in the present study not only enhances the mechanical property of PMMA/wood-based materials (stronger than PMMA materials) but also serves as oxygen barrier to protect dopant's triplet excited states from oxygen quenching (unlike PMMA-based materials, the RTP afterglow property of dopant-PMMA/wood materials can be activated by short-term excitation). This interesting combination of polymer, wood, and room-temperature phosphorescence has resulted in long afterglow emission lifetime, excellent functionality, and important practical significance.

Results

Design and synthesis of BF_2bdk luminescent dopants for afterglow material fabrication

It is known that materials' afterglow brightness at time, t, after ceasing excitation light can be expressed as $L(t) \sim \varepsilon\Phi e^{-t/\tau}$, where ε, Φ and τ represent molar absorption coefficient, afterglow efficiency and afterglow lifetime, respectively[83,84]. $L(t)$ increases with ε, Φ and τ. BF_2bdk compounds are selected as luminescent dopants to prepare RTP afterglow materials in the present study because of the following reasons. (1) In the aspect of ε, many BF_2bdk molecules possess large ε. Here **2 F** and **23 F** molecules exhibit ICT characters in their S_1 states (Fig. 1) and show large ε around $2 \sim 3 \times 10^4\ M^{-1}\ cm^{-1}$ in UVA region (Supplementary Table 1). (2) For intersystem crossing (ISC), it is noted that the multiple electron-donating functional groups on **2 F** and **23 F** molecules enrich the types of both singlet and triplet excited states. As a result, some triplet excited states would have different excited state natures from S_1 states, which would enhance S_1-to-T_n ISC process according to the El-Sayed rule. This receives the support from TD-DFT calculation where multiple ISC channels between S_1 and T_n states with moderate or large SOCME values (around or $>0.5\ cm^{-1}$) can be found (Fig. 1 and Supplementary Fig. 1–2). Besides, dipole-dipole interaction between ground-state matrix and S_1-state BF_2bdk also increase ISC tendency in the system (*vide infra*). High ISC quantum yield represents a prerequisite for high afterglow efficiency. (3) In the aspect of τ_P, in the absence of heavy atom effect and strong n-π* transition characters, BF_2bdk's T_1 states show small phosphorescence rates (k_P) and can exhibit long phosphorescence lifetimes (τ_P) when nonradiative decay and oxygen quenching are sufficiently suppressed under ambient conditions.

Here the BF_2bdk compounds (**2 F** and **23 F**) were synthesized using the Suzuki-Miyaura reaction and our cascade reaction; aromatic intermediates were formed by the reaction of bromo triphenylbenzene with 4-methoxyphenylboronic acid, followed by

https://doi.org/10.1038/s41467-025-55990-z

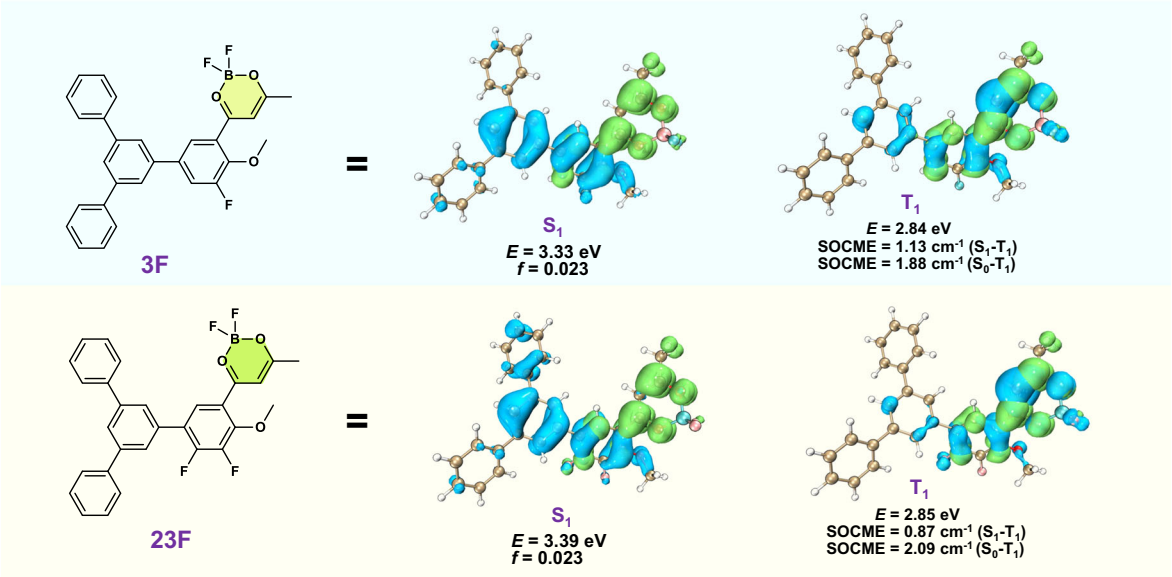

Fig. 1 | Structures and properties of BF_2bdk. Isosurface maps of electron-hole density difference of the lowest singlet and triplet excited states of **3 F** and **23 F** obtained by TD-B3LYP/6-31 g(d,p).

stirring with boron trifluoride etherate ($BF_3{\cdot}Et_2O$) and acetic anhydride at 85 °C for 4 h to yield the final BF_2bdk compounds (see Methods and Supplementary Methods). To isolate the BF_2bdk compounds, column chromatography was performed on silica gel, followed by recrystallization for purification. The purity of the compound was confirmed by HPLC, and their structures were characterized using ^{1}H NMR, ^{13}C NMR, and ^{19}F NMR spectra (Supplementary Fig. 3-14). Detailed information regarding the synthetic procedures, structural characterization, and purity of the BF_2bdk compounds can be found in Supplementary Information.

We characterized compounds **3 F** and **23 F**, and the results showed that both compounds exhibited high-energy absorption bands at 250–300 nm and low-energy absorption bands at 300–400 nm in dichloromethane solution, as well as similar absorption band shapes and absorption maxima in other common organic solvents according to their UV-vis spectra (Supplementary Fig. 15 and Supplementary Table 1). As supported by TD-DFT calculations, which indicated that compounds **3 F** and **23 F** could be assigned to ICT transitions from the triphenyl to the dioxaborine group (Fig. 1). However, solutions or powders of **3 F** and **23 F** do not exhibit afterglow under environmental conditions (Supplementary Fig. 16). This can be attributed to two factors: (a) the intersystem crossing tendency is not strong enough to form sufficient triplets in single-component BF_2bdk system; (b) the active intramolecular motion (in solution state) and the electronic coupling between neighboring molecules (in powder) contribute the nonradiative decay of triplet excited states and thus quenching room temperature phosphorescence[57,83].

Material fabrication and photophysical measurements

We prepare RTP transparent wood according to the procedure as shown in Fig. 2a; transparent wood, which inherently possesses multifunctionality, can also serve as the polymer matrix for BF_2bdk (Fig. 2). Based on our previous research, PMMA was used as the matrix and doped with BF_2bdk compounds to design high-performance organic afterglow systems, providing beneficial assistance in their applications[50–57,71,80,82]. We doped compounds **3 F** and **23 F** to prepare **3F**-PMMA and **23F**-PMMA samples, and found that the afterglow duration of the two polymer-based materials can last for 8–9 s at room temperature (Fig. 2c, e). And the τ_P is between 800 and 1000 ms (Fig. 2h, i, l, m). In order to investigated the triplet excited state properties of compounds **3 F** and **23 F** when doped in transparent wood matrix, we doped the same concentration of BF_2bdk into MMA during the preparation of transparent wood, resulting in transparent wood samples with yellow-green afterglow at room temperature (Fig. 2b, d). The steady-state emission spectrum of the **3F**-PMMA/wood sample showed fluorescence bands in the range of 385–500 nm, with a maximum emission wavelength of 414 nm (S_1 level, 3.33 eV). The delayed emission spectrum (1 ms delay) displayed phosphorescent bands in the range of 500-650 nm (Fig. 2f), with the maximum emission peak at 524 nm (T_1 level, 2.84 eV). The PLQY of the **3F**-PMMA/wood sample was 29%. The emission decay curve monitored at 524 nm revealed a τ_P of 1023.9 ms for the solid sample of **3F**-PMMA/wood (Fig. 2g). **23F**-PMMA/wood samples exhibit typical RTP performance similar to **3F**-PMMA/wood. The steady-state emission spectrum of the **23F**-PMMA/wood sample showed the maximum emission spectrum at 408 nm (S_1 level, 3.39 eV), while the delayed emission spectrum (1 ms delay) displayed phosphorescent bands in the range of 480-600 nm (Fig. 2j), with the maximum emission peak at 515 nm (T_1 level, 2.85 eV). The PLQY of the **23F**-PMMA/wood sample reached 35%. The τ_P of the **23F**-PMMA/wood sample was 1035.3 ms (Fig. 2k). Compound **23 F** in the PMMA/wood matrix exhibited similar afterglow properties to the **3F**-PMMA/wood sample, which is consistent with the observed electron-hole diagram of their T_1 states (Fig. 1).

To confirm that both **3 F** and **23 F** exhibit RTP-type afterglow mechanisms, energy transfer, donor-acceptor afterglow, and impurity-induced mechanism, all of which have the potential to induce afterglow property, have been unambiguously ruled out. (1) Room-temperature afterglow can be induced by excited-state energy transfer from RTP donors to emitting acceptors[85,86], and the energy transfer process only occurs when the donor is sufficiently excited. The BF_2bdk-PMMA/wood afterglow materials obtained in this study can be excited by 365 nm UV light, whereas PMMA/wood matrix shows negligible UV-vis absorption at 365 nm (Supplementary Fig. 17). Besides, PMMA/wood sample (without BF_2bdk) has insignificant room-temperature afterglow upon ceasing 365 nm excitation (Supplementary Fig. 18). Therefore, the possibility of room temperature afterglow induced by energy transfer from the PMMA/wood matrix to BF_2bdk can be ruled out. (2) Recent studies have shown that when the T_1 energy levels of the organic matrix fall between the S_1 and T_1 states of the dopant, the T_1 state of the organic matrix can act as a bridge for the

https://doi.org/10.1038/s41467-025-55990-z

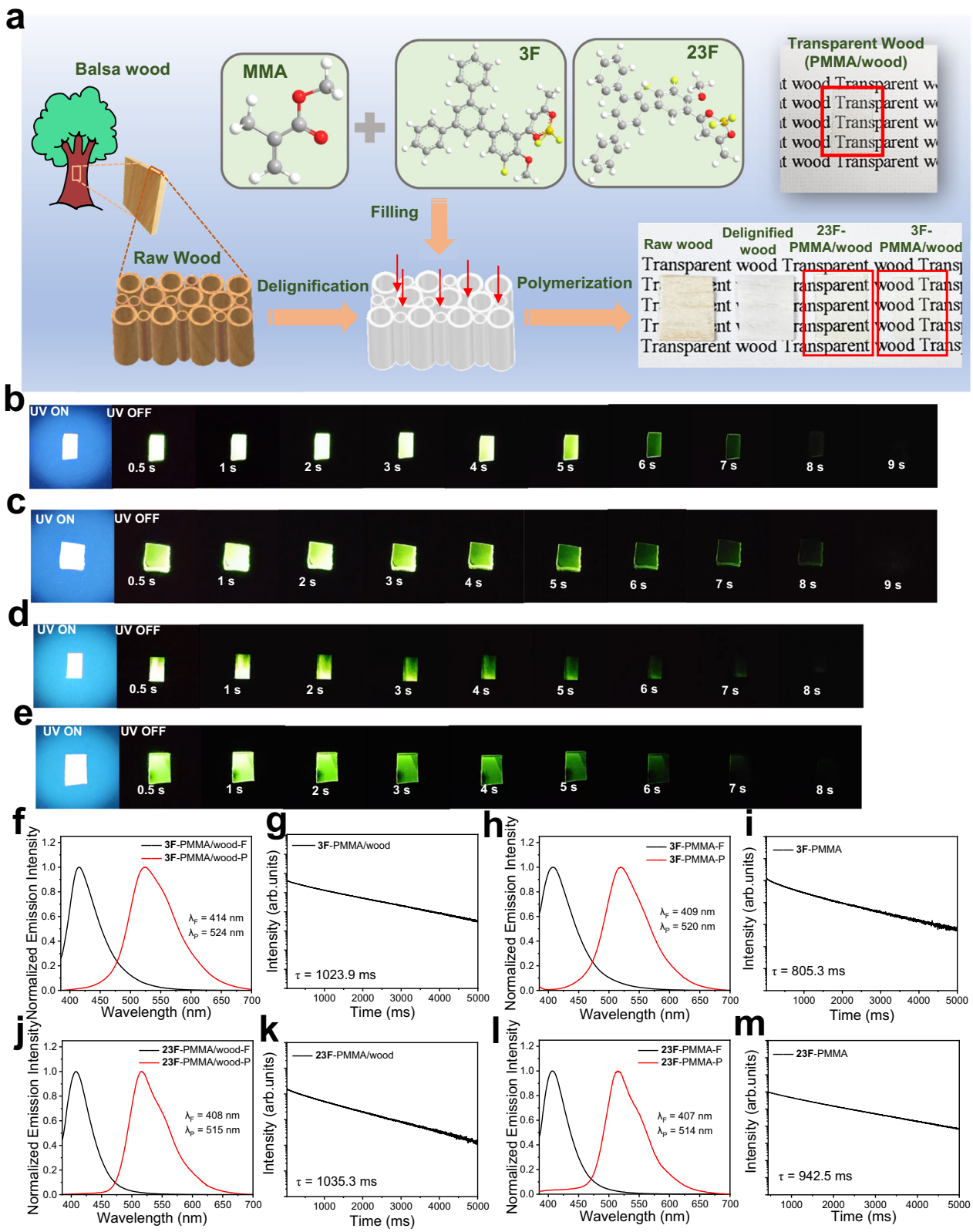

Fig. 2 | Preparation and photophysical properties of BF_2bdk-PMMA and BF_2bdk-PMMA/wood system. a Schematic illustration of the preparation of RTP transparent wood; Photographs of (**b**) **3F**-PMMA/wood, (**c**) **3F**-PMMA, (**d**) **23F**-PMMA/wood and (**e**) **23F**PMMA samples at UV-ON and UV-OFF states; room-temperature steady-state and delayed emission spectra of (**f**) **3F**-PMMA/wood, **h** **3F**-PMMA, **j** **23F**-PMMA and (**l**) **23F**-PMMA; room-temperature phosphorescence decay of (**g**) **3F**-PMMA/wood, (**i**) **3F**-PMMA, (**k**) **23F**-PMMA/wood and (**m**) **23F**-PMMA.

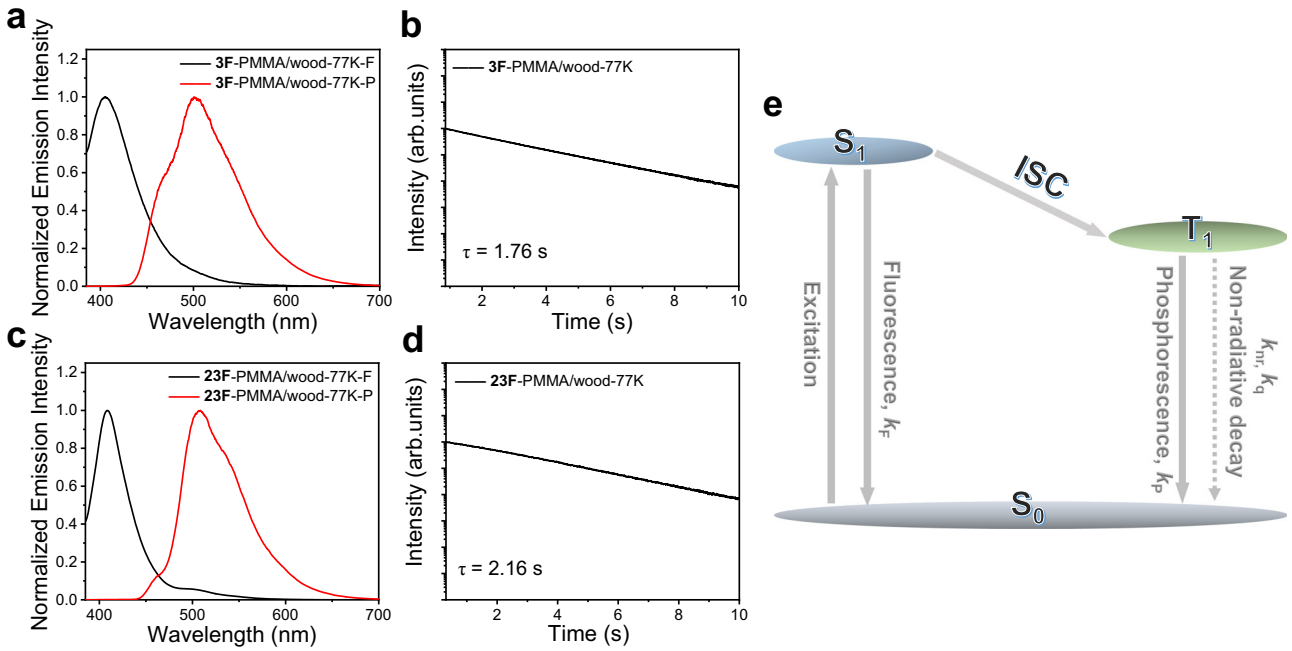

Fig. 3 | Photophysical properties of RTP transparent wood at 77 K and the proposed RTP mechanism. 77 K delayed emission spectra of (**a**) **3F**-PMMA/wood and (**c**) **23F**-PMMA/wood; 77 K emission decay profile of (**b**) **3F**-PMMA/wood and (**d**) **23F**-PMMA/wood; (**e**) Proposed RTP mechanism of BF_2bdk-PMMA/wood materials.

intersystem crossing (ISC) from singlet to triplet states of the dopant, leading to the occurrence of organic room-temperature afterglow[87]. The T_1 energy levels of PMMA and cellulose and hemicellulose of delignified wood have been estimated from their units (Supplementary Fig. 19 and Supplementary Table 2) to be 5.11 eV, 6.67 eV and 6.87 eV by TD-B3LYP/6-31 G(d, p), respectively (it is difficult for us to obtain PMMA and delignified wood's T_1 levels by experiments due to their insignificant phosphorescence). As a result, the ISC-bridged process is not applicable to the BF_2bdk-polymer system in this study, as the T_1 level of the PMMA/wood matrix is significantly higher than the S_1 and T_1 states of the BF_2bdk molecules (around 3.35 eV and 2.85 eV obtained from fluorescence and phosphorescence maxima). Additionally, the high T_1 level of the organic matrix plays a crucial role in preventing afterglow quenching caused by triplet-to-triplet energy transfer from the luminescent dopant to the organic matrix, enabling the construction of high-performance afterglow materials[88]. (3) In organic materials, the donor-acceptor mechanism can induce charge separation states, which has been observed in some organic systems[58,59]. Long-lived luminescence observed in organic systems is attributed to retarded charge recombination in rigid solid matrices. For organic donor-acceptor afterglow systems, the formation of charge separation states through intermolecular charge transfer between donor and acceptor molecules is a prerequisite for long-lasting luminescence. However, in this study, negligible intermolecular charge transfer between the BF_2bdk dopant and the organic matrix was observed due to the lower HOMO and higher LUMO levels of the latter (the HOMO/LUMO levels of BF_2bdk, PMMA unit and delignified wood unit have been summarized in Supplementary Table 2), excluding the possibility of a long-lasting luminescence mechanism in this system. (4) Recent reports suggest that impurities may also be a possible cause of organic room temperature afterglow[89]. In this study, careful purification of the BF_2bdk compound was carried out using column chromatography, followed by three recrystallizations in spectroscopic grade dichloromethane/hexane to ensure its purity. Additionally, HPLC confirmed their high purity (Supplementary Fig. 20). The obtained high-purity BF_2bdk powder did not exhibit afterglow properties at room temperature. However, the afterglow material obtained by doping BF_2bdk into a host matrix showed significant afterglow properties under ambient conditions. It is worth noting that the afterglow material obtained at low doping concentrations still exhibited high-performance afterglow characteristics. In the low-concentration afterglow material, even if there are possible impurities, the BF_2bdk molecules and any potential impurities should be separated by the organic matrix, so that the charge separation and recombination processes between the BF_2bdk molecules and any possible impurities can be statistically negligible. We also compare excitation spectra and UV-vis spectra of the system (Supplementary Fig. 15 and 20). The UV-vis spectra show electronic absorption property of luminescent dopants, while the excitation spectra reveal the absorption property of luminescent component in the system. The match between UV-vis and excitation spectra supports that the luminescent property of the present system comes from BF_2bdk dopants rather than impurity. These experimental and analytical results presented in this article exclude the possibility that impurities cause the room-temperature afterglow performance.

We investigated the delayed emission at 77 K and found that low temperature prolongs the phosphorescence lifetime, which is a typical RTP mechanism. At 77 K, the **3F**-PMMA/wood and **23F**-PMMA/wood materials exhibit a peak at about 408 nm in their steady-state emission, with a delayed emission spectrum (1 ms delay) of 507 nm (Fig. 3a–d), consistent with those at room temperature. So, the room-temperature phosphorescence and delayed emission of BF_2bdk-PMMA/wood originate from the slow phosphorescence decay of the T_1 state of BF_2bdk in the PMMA/wood matrix (Fig. 3e). According to previous studies, the polymer matrix can simultaneously lower k_F and increase k_{ISC} of the ICT state through dipole-dipole interactions, significantly promoting the ISC of the BF_2bdk excited state[51,52,56]. Here we perform photophysical measurements of BF_2bdk in polystyrene (PS), poly(methyl methacrylate) (PMMA), phenyl benzoate (PhB) and 4-methoxybenzophenone (MeOBP) (Supplementary Fig. 21 and 22) and calculate the dipole moments of ground-state matrices and S_1-state BF_2bdk (Table 1) to investigate the dipole-dipole interaction for ISC enhancement. Steady-state emission spectra (Supplementary Fig. 21) exhibit that the fluorescence maxima (λ_F) of **3F**-matrix samples increase with the dipole moments of organic matrices (Table 1). Delayed emission spectra show less significant change of

Table 1 | Photophysical data of 3 F in different organic matrices by experiment and dipole moment of the ground-state organic matrices by TD-DFT calculation

Entry	λ_F (nm)	λ_P (nm)	S_1 (eV)	T_1 (eV)	Dipole moment of ground-state matrix (Debye)	ΔE_{ST} (eV)
3F-PS	413	531	3.00	2.34	0.4580	0.66
3F-PMMA	412	524	3.01	2.37	1.6943	0.64
3F-PhB	422	522	2.94	2.38	1.9406	0.56
3F-MeOBP	436[a]	522	2.84	2.38	2.8802	0.46

[a]obtained from delayed emission spectra (the delayed fluorescence band at 436 nm) since the steady-state emission spectra are strongly interfered by MeOBP's emission.

phosphorescence maxima upon the variation of organic matrices (Supplementary Fig. 21). These suggest that the organic matrices interact with S_1-state **3 F** molecules via dipole-dipole interaction and thus lower **3 F**'s S_1 level; the dipole moment of **3 F**'s S_1 state can be calculated by TD-DFT to be 5.97 Debye. **3 F**'s T_1 level is found to be insensitive to the medium (Table 1), which obey Kasha's exciton model[90]. Consequently, the decrease of singlet-triplet splitting energy (ΔE_{ST}) leads to ISC enhancement in organic matrices with larger dipole moments. To further investigate ISC behavior, excited state lifetimes of **3 F**'s S_1 states (τ_F) have been measured from fluorescence decay profiles (Supplementary Fig. 22). The average τ_F has been found to first increase with matrix's ground-state dipole moments from PS (2.0 ns) through PMMA (2.3 ns) to PhB (3.8 ns) and then decrease to 1.9 ns in MeOBP matrix (Supplementary Fig. 22). According to the reported studies on τ_F of ICT systems[51,52,91–93], fluorescence decay rate constant (k_F) decreases with the polarity of the medium, which can explain τ_F increase from PS through PMMA to PhB. In view of the equation $\tau_F = 1/(k_F + k_{ISC} + k_{nr})$ (k_{ISC} and k_{nr} represent ISC and nonradiative decay rate constants, respectively), the decrease of τ_F to 1.9 ns suggest significant enhancement of k_{ISC} in MeOBP matrix with large dipole moment (Table 1). Given $\Phi_{ISC} = k_{ISC}/(k_F + k_{ISC} + k_{nr})$, the simultaneous k_{ISC} increase and k_F decrease upon dipole-dipole interaction between ground-state matrices and S_1-state BF_2bdk can significantly boost Φ_{ISC} in the RTP system. This is our understanding of the role of organic matrix for emergence of organic afterglow in the present system; recent studies based on ultrafast spectroscopy[94] support our proposed dipole effect for ISC enhancement. It should be noted that, despite their strong capability in Φ_{ISC} enhancement, PhB and MeOBP are small-molecule matrices that are not suitable for fabricating transparent wood.

In control experiment, we have prepared RTP wood using natural wood as a template and also performed photophysical studies on the obtained RTP wood. The fluorescence and phosphorescence bands of **23F**-PMMA/raw wood (RTP wood, not transparent) are similar to those of **23F**-PMMA/wood (i.e. the RTP transparent wood). However, the RTP lifetime of **23F**-PMMA/raw wood (568.6 ms) has been found to be shorter than that of **23F**-PMMA/wood (1035.3 ms) (Supplementary Fig. 23). UV-Vis spectra collected by an integrating sphere system show that the delignified wood (obtained by $NaClO_2$ treatment) and bleached wood (obtained by Hu's H_2O_2/UV method) have insignificant or weaker absorption in the visible region. In contrast, raw wood has significant absorption in the 420-700 nm visible region in its UV-vis spectrum (Supplementary Fig. 24); this visible absorption property is attributed to the chromophore groups in lignin. Given the spectral overlap between **23F**-PMMA's phosphorescence band and raw wood's absorption band in the visible region, the decrease of RTP lifetime of **23F**-PMMA/raw wood (568.6 ms, when compared to **23F**-PMMA/wood's RTP lifetime of 1035.3 ms) can be attributed to excited state energy transfer from **23 F**'s T_1 states to lignin's chromophore groups in raw wood[86]. In the RTP transparent wood system where delignified wood is used, such excited state energy transfer should be insignificant, so the organic triplet excited states keep long phosphorescence lifetimes; this is an additional advantage of using transparent wood as organic matrix for preparing RTP materials.

Structure and property of RTP transparent wood

The characterization of the transparent wood was conducted (Fig. 4). In the FT-IR spectra, the characteristic band at 1505 cm^{-1} corresponded to the aromatic skeleton vibration of lignin, which is attributed to the presence of phenolic aldehyde hydroxyl groups (Fig. 4j)[95]. However, in the spectrum of PMMA/wood, the characteristic peaks of lignin disappeared, while the carbonyl (C = O) band of PMMA appeared, further confirming the successful combination of the two components. SEM observation shows the filled and unfilled structures of wood in both longitudinal and cross-sectional directions (Fig. 4a–d), ensuring that the wood is well infiltrated, which is consistent with the reported structure of transparent wood. SEM/elemental mapping exhibits the distribution of fluorine element on the cross section of BF_2bdk-PMMA/wood RTP materials (fluorine is exclusively from BF_2bdk, Fig. 4e–h), from which one can find BF_2bdk molecules are well dispersed in the materials. The loading content of BF_2bdk has been measured by UV-vis method based on Lambert-Beer law to be ~0.23 wt% in BF_2bdk-PMMA/wood materials (PMMA and BF_2bdk in BF_2bdk-PMMA/wood materials can be readily dissolved in dichloromethane. BF_2bdk has significant absorption in UVA region while PMMA doesn't). We also perform ultrathin cross-sectional TEM observation and XRD measurement to further study the morphology and structure of natural wood and transparent wood. Before TEM analysis, the samples are stained by uranyl acetate and lead citrate. Figure 4l show the ultrastructure of the wood cell wall, similar to the reported studies[96]. For the sample of transparent wood (Fig. 4m), the framework structure with higher contrast can be assigned to the wood frame, while the component with lower contrast can be attributed to PMMA within the wood frame. In control experiments, BF_2bdk-PMMA materials show room-temperature afterglow after sufficient UV irradiation (Fig. 2c, e), whereas BF_2bdk-delignified wood samples show very weak afterglow at room temperature (Supplementary Fig. 25). These suggest that the afterglow property of BF_2bdk-PMMA/wood materials mainly originates from the BF_2bdk molecules in PMMA domains (Fig. 4i). The rigid microenvironment provided by the glassy polymer matrix (PMMA polymers in transparent wood materials have number-averaged molecular weight (M_n) of 226 kg/mol, weight-averaged molecular weight (M_w) of 523 kg/mol, and a polydispersity index (M_w/M_n) of 2.31 (Supplementary Fig. 26), as measured by GPC in tetrahydrofuran phase using polystyrene standard) can restrict the non-radiative deactivation of the BF_2bdk triplet state and to some extent protect the triplet state from oxygen quenching. It is known that PMMA matrix allows oxygen permeation[74–77], especially in the film state. Under ambient conditions, the organic afterglow properties of PMMA-based materials typically cannot be activated by short-term and low-power excitation because oxygen in the PMMA matrix can quench the triplet excited states of the luminescent dopants[74–77]. After sufficient irradiation, oxygen in the PMMA matrix can be removed and activated, exhibiting obvious room-temperature phosphorescence. Interestingly, when PMMA is combined with wood, RTP of BF_2bdk-PMMA/wood materials can be generated under short-term excitation, compensating for the shortcomings of pure PMMA as a matrix. Cellulose and hemicellulose in the wood, which are rich in hydroxyl groups, can form multiple short and strong hydrogen bonds (confirmed by FT-IR as shown in Fig. 4j) to serve as oxygen barriers; cellulose fibrils have long been known as an excellent oxygen barrier because of hydrogen bonding and relatively high crystallinity[97]. Fig. 4k show that raw wood, delignified wood, and PMMA/wood show characteristic diffraction peaks at 15.8° and 22.3° in the XRD profiles (λ = 0.154 nm, Cu-Kα radiation), which can be assigned to (101) and (002) planes of type I crystalline cellulose, respectively[98]. The XRD studies indicate that the delignification and

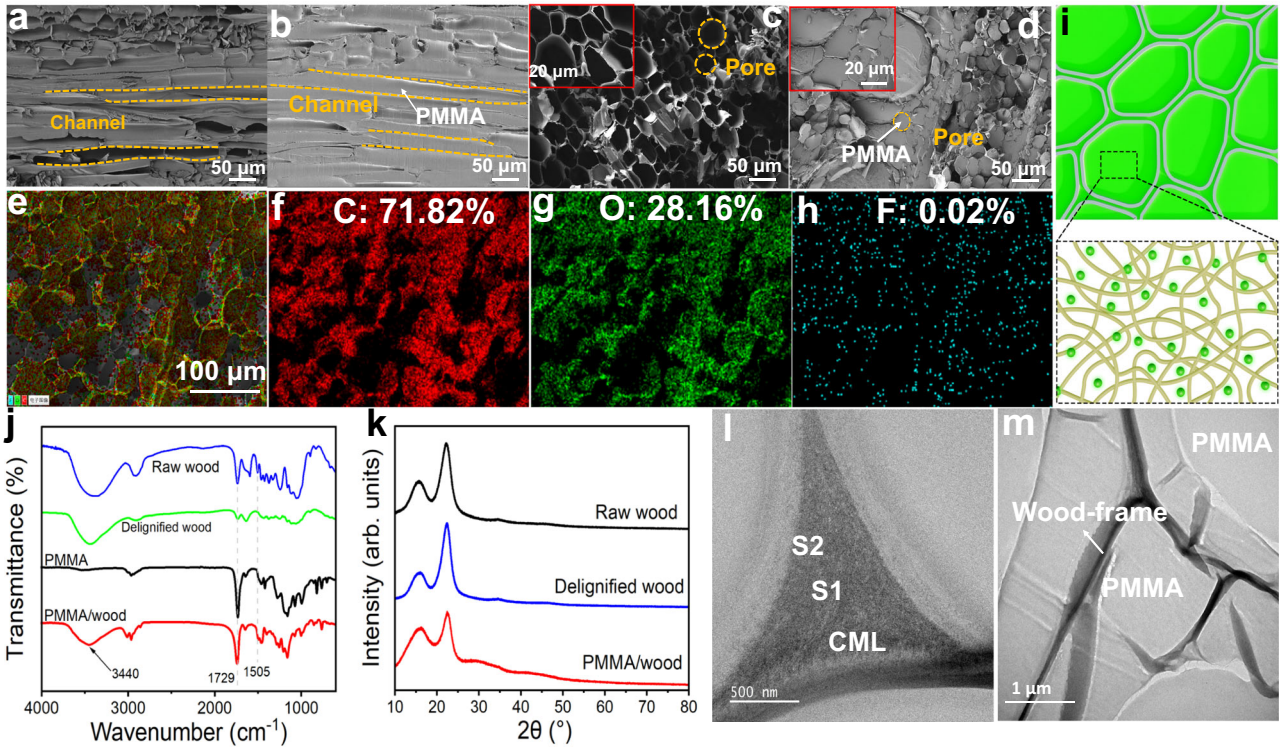

Fig. 4 | Structure of transparent wood. Longitudinal-sectional SEM images of (**a**) raw wood and (**b**) **23F**-PMMA/wood; Cross-sectional SEM images of the (**c**) raw wood and **d** **23F**-PMMA/wood; (**e**–**h**) SEM/elemental mapping of **23F**-PMMA/wood (carbon, oxygen and fluorine); (**i**) Scheme of the morphology and structure of BF_2bdk-PMMA/wood; (**j**) FT-IR of raw wood, delignified wood, PMMA and PMMA/wood; (**k**) XRD of raw wood, delignified wood and PMMA/wood; Ultrathin cross-sectional TEM images of (**l**) raw wood and (**m**) **23F**-PMMA/wood.

transparent wood production processes didn't disrupt the crystalline structure of cellulose. These results, together with SEM and TEM observations in Fig. 4, indicate that the PMMA micro-domains are encapsulated by the wood frame (Fig. 4i), and wood frame composed of crystalline cellulose with rich hydrogen bonding can serve as oxygen barrier to suppress oxygen quenching of organic triplets in the transparent wood system, thereby improving afterglow performance. Since the PMMA micro-domains are encapsulated by these wood frame, the oxygen diffusion within the PMMA/wood materials would be largely suppressed. Given the $k_{nr} + k_q$ values at 77 K are negligibly small, experimental k_P values can be estimated from τ_P at 77 K to be 0.57 and 0.46 s^{-1} for the **3 F** and **23 F** systems, respectively. According to the equation $\tau_P = 1/(k_P + k_{nr} + k_q)$, experimental $k_{nr} + k_q$ values in transparent wood at room temperature can be calculated to be as small as 0.41 and 0.51 s^{-1} for the **3 F** and **23 F** systems, respectively. The collaboration of PMMA and wood for the protection of organic triplet excited states lays a solid foundation for the development of room-temperature organic afterglow transparent wood as a biomass-based type of material.

The transmittance of the PMMA/wood and BF_2bdk-PMMA/wood composite materials at 550 nm both were 92% (Fig. 5a) and haze value of these exceeded 86% (Fig. 5b). The high transmittance of PMMA/wood ensured the effective collection of light, while the high haze enlarged the irradiation area of light under the same lighting conditions. Compared to glass materials, which have almost no light scattering ability, PMMA/wood was more flexible in the use of light. This capability was meaningful for the construction of indoor lighting buildings, which could achieve a uniform lighting. Particularly, the high haze obscuration effect becomes prominent when the distance between the object and PMMA/wood is >5 cm (Fig. 5c).

The mechanical property of the transparent wood has also been tested. The maximum tensile strength and modulus of elasticity (MOE) of the raw wood in the longitudinal direction were 10.53 MPa and 2289.57 MPa, respectively. The PMMA/wood composite materials exhibited values of 64.92 MPa and 4083.16 MPa, respectively (Fig. 6a, b). In PMMA/wood composite materials, the rigid structural lignin is removed, and the presence of hemicellulose is considered crucial for forming a rigid network of interconnected cells. This is due to the high retention of hemicellulose components in the wood matrix, which cover the surface of cellulose microfibers, improving the bonding between fibers and forming a rigid hydrogen bonding network with cellulose and filled PMMA to support the cell wall[1–15]. According to the reported study of compressed wood prepared in the literature[6], the tensile stress of transparent wood can be significantly enhanced by increasing the cellulose volume fraction. Here we also increased the cellulose volume fraction from 5%–20% by wood compressing to obtain a tensile stress of 149 MPa (Supplementary Fig. 27). In addition, PMMA/wood had an initial instantaneous water contact angle of 91° and stabilized after 30 s, indicating its good hydrophobicity (Fig. 6c). Therefore, PMMA/wood is a promising material with strong vitality and good industrial prospects in the field of high-performance polymers. We also tested the water absorption thickness expansion rate of PMMA/wood after soaking in water for 24 h, and almost no deformation occurred, indicating that it has good dimensional stability (Supplementary Table 3). Through thermogravimetric analysis (TGA), it can be seen that transparent wood also has good heat resistance compared to raw wood (Supplementary Fig. 28). Finally, we observed the chemical resistance of three groups of transparent wood samples by treating them in a 5% H_2SO_4 solution, a 4% NaOH solution for 48 h, and a 3% NaCl aqueous solution for 24 h. Due to the acid, alkali, and salt resistance of PMMA itself, which is filled into the wood frame, it has a good protective effect on wood. As a result, transparent wood didn't undergo any changes, such as foaming or corrosion (Supplementary Fig. 29). To investigate the durability of the materials,

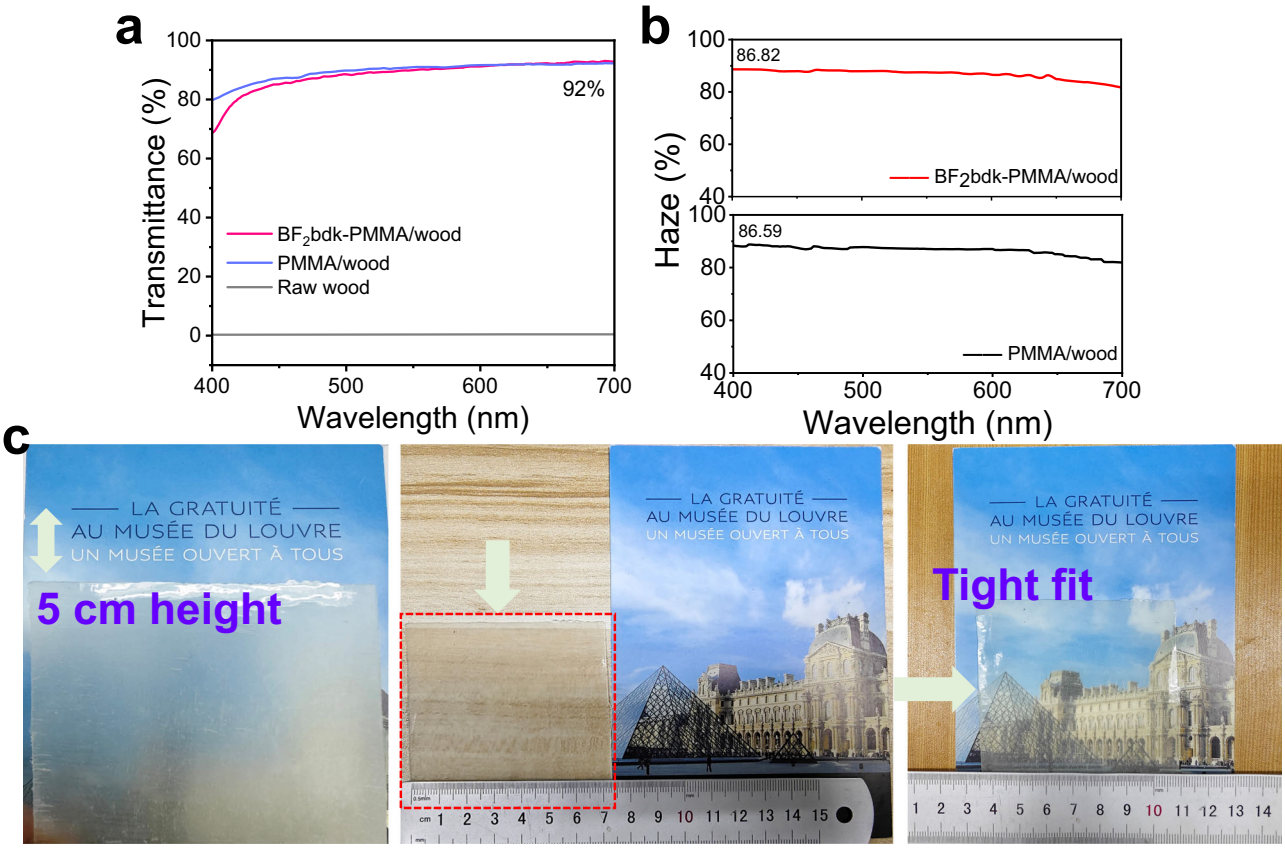

Fig. 5 | Property of transparent wood. a Transmittance and (**b**) haze of PMMA/wood, PMMA and raw wood; (**c**) Photographs of a 7 cm × 7 cm × 0.5 mm transparent wood at a height of 5 cm (left), transparent wood closely fitting the pattern next to it (middle) and closely matches the pattern (right).

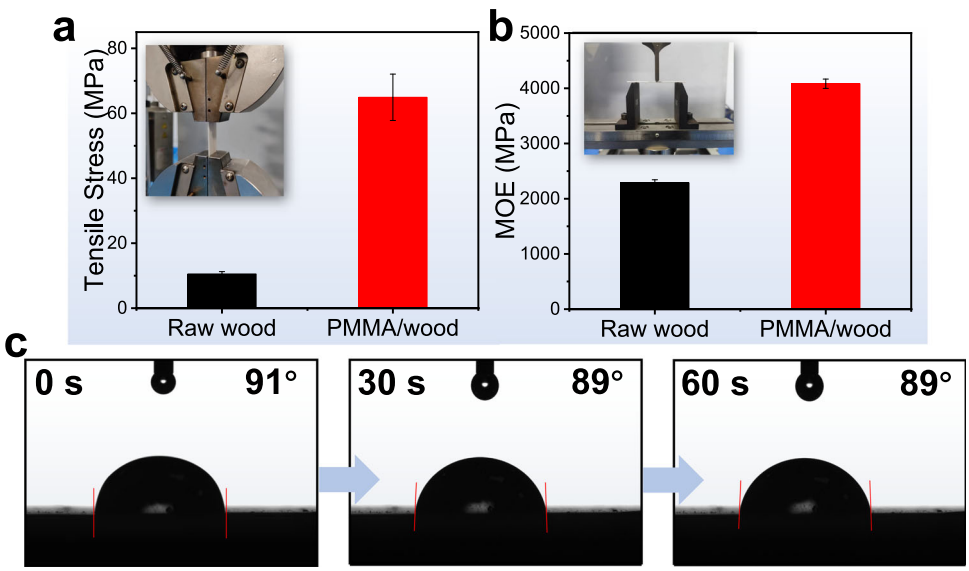

Fig. 6 | Mechanical and hydrophobic properties of transparent wood. a Tensile stress and (**b**) MOE of raw wood and PMMA/wood (standard deviation is given); (**c**) Water contact angle of PMMA/wood at 0 s, 30 s and 60 s.

corresponding experiments have been performed: (1) the materials are exposed to a xenon lamp with a power density of about 90 mV/cm^2 (to simulate sunlight) for 12 h; (2) the materials are placed in a 65% ± 5% humidity box at 20 ± 2 °C for 12 h; (3) to accelerate the experiment of thermal stability, the materials are placed in an 80 °C oven for 1 h. After these treatments, the mechanical property (tensile strength and MOE) and afterglow property (τ_P) have been found to show only small change (Supplementary Fig. 30), indicating the durability of the materials. Such kind of materials does indeed have excellent durability as reported in the literature[18,98,99].

Universality of the method

In addition to BF_2bdk compounds, other luminescent dopants such as coronene (Cor) with a strong ISC tendency and a small k_P value[100–102]

have also been introduced to the transparent wood system. Different from the ICT character of BF_2bdk system, coronene's S_1 and T_1 states are of localized excitation (LE) character. Unlike many aromatic compounds, coronene molecules of D_{6h} symmetry feature symmetry-forbidden S_1-to-S_0 transition, exhibit fluorescence lifetime (τ_F) up to around 100 ns in rigid environment, and possess fluorescence decay rate (k_F) on the order of only $10^6\ s^{-1}$[103]. According to the equation $\Phi_{ISC} = k_{ISC}/(k_F + k_{ISC} + k_{nr})$, the small k_F is conducive for coronene system to obtain a high Φ_{ISC}, which represents a prerequisite for bright RTP materials. In addition, coronene's T_1-to-S_0 transition is spin-forbidden and symmetry-forbidden, so that its k_P is as small as ~0.1 s^{-1}[100–102]. In this study, coronene was used as luminescent dopant dissolved in MMA to prepare room-temperature organic afterglow transparent wood (Fig. 7). The steady-state emission spectrum of Cor-PMMA/wood showed fluorescence bands in the range of 400–500 nm (Fig. 7f), while the delayed emission spectrum displayed characteristic phosphorescent bands of coronene in the range of 500–650 nm, with the maximum emission at 566 nm. Cor-PMMA and Cor-PMMA/wood exhibited the same trend (Fig. 7d), and in the PMMA/wood matrix, the duration of organic afterglow at room temperature is 20 s, which is longer than what was observed in Cor-PMMA (Fig. 7a, b), while the τ_P is 0.8 s longer (Fig. 7e, g). When coronene's T_1 states are well protected in PMMA/wood matrix, the luminescent system exhibits bright RTP with τ_P of 4.1 s (Fig. 7g). In addition, we also perform deuteration on coronene molecules. C-D bond vibration is much weaker than that of C-H bond, so that the intramolecular motion of DCor's T_1 states would be suppressed. The DCor-PMMA/wood RTP materials have been found to show brighter afterglow and longer τ_P up to 11.9 s (Fig. 7c, f, g).

More wood species have been tried. We use delignified pine, poplar, ash and beech in the place of delignified balsa wood to prepare BF_2bdk-PMMA/wood samples. Despite the obtained samples exhibit similar fluorescence and phosphorescence bands to balsa system, the obtained samples show much lower transparency than balsa system (Supplementary Fig. 31). The reduced transparency should be caused by the increased wood density[104]; pine, poplar, ash and beech have higher density than balsa wood.

Besides Berglund's pioneering method for conventional preparation of transparent wood[6], we also use Hu's H_2O_2/UV method[1] to remove lignin's chromophores and then perform infiltration to prepare dopant-PMMA/wood RTP materials (size, 22 cm × 8 cm), which would be time-saving and cost-effective and can reduce the amount of liquid waste. The transparency and afterglow property are similar to that obtained by conventional method (Supplementary Fig. 32). Due to the limited size of vacuum impregnation setup in our institute, currently we are unable to perform large-scale fabrication. Despite of this, we still propose and illustrate the process for large-scale preparing RTP transparent wood (Supplementary Fig. 33). In the future, we will perform large-scale fabrication for applications. In addition, the preparation of thicker transparent wood (2 mm and 3 mm) has also been carried out (Supplementary Fig. 34).

Material functions

In previously reported studies on the preparation of polymer-based afterglow materials, luminescent objects were manufactured using solution-casting techniques, which required the evaporation of solvents and caused significant environmental harm. In this study, we can create organic afterglow materials with various shapes by designing the shape of the wood (Fig. 8a). Inspired by recent studies using the indirect strategy of excited-state energy transfer[27,85,86,105], we used Cor-PMMA/wood as the donor and selected rhodamine 6 G (R6G) as the acceptor to prepare three-component Cor-PMMA/wood-R6G samples, which inherited the strong phosphorescence and longer afterglow duration of the Cor-PMMA/wood donor (observable for up to 21 s with human eyes) (Fig. 8b). The steady-state emission spectrum of the Cor-PMMA/wood-R6G three-component sample showed combined emission from Cor-PMMA/wood and R6G, while the delayed emission spectrum displayed emission at 571 nm and 634 nm (Fig. 8e, f). Although the triplet-to-singlet energy transfer from coronene to R6G is spin-forbidden, resulting in a small rate constant (k_{ET}), the small k_P and long τ_P of the coronene triplet state provide sufficient opportunity for triplet-to-singlet energy transfer, thereby achieving excited-state energy transfer from Cor-PMMA to R6G fluorescent dye. In addition,

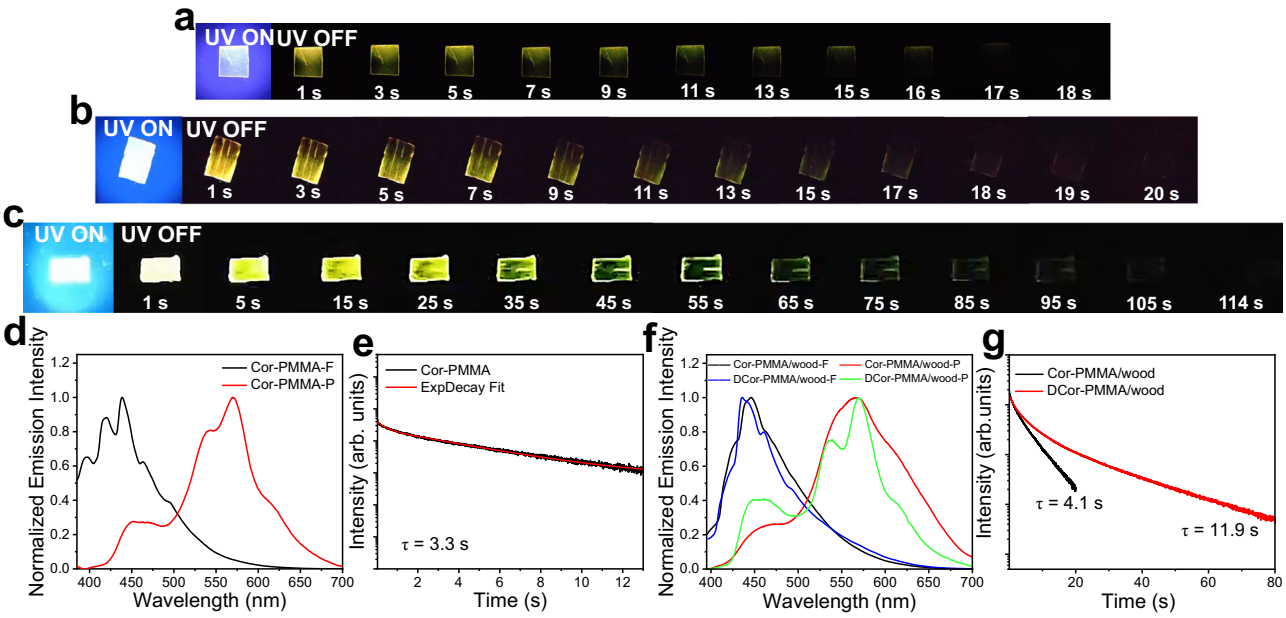

Fig. 7 | Photophysical property of coronene transparent wood systems. Photographs of (**a**) Cor-PMMA, (**b**) Cor-PMMA/wood and (**c**) DCor-PMMA/wood materials at UV-ON and UV-OFF states; (**d**) Room temperature steady-state emission spectra and delayed emission spectra (1 ms delay) of Cor-PMMA; (**e**) The emission decay curves of Cor-PMMA under ambient conditions monitored at 570 nm; (**f**) Room temperature steady-state emission spectra and delayed emission spectra (1 ms delay) of Cor-PMMA/wood and DCor-PMMA/wood; (**g**) The emission decay curves of Cor-PMMA/wood and DCor-PMMA/wood materials under ambient conditions monitored at 570 nm.

https://doi.org/10.1038/s41467-025-55990-z

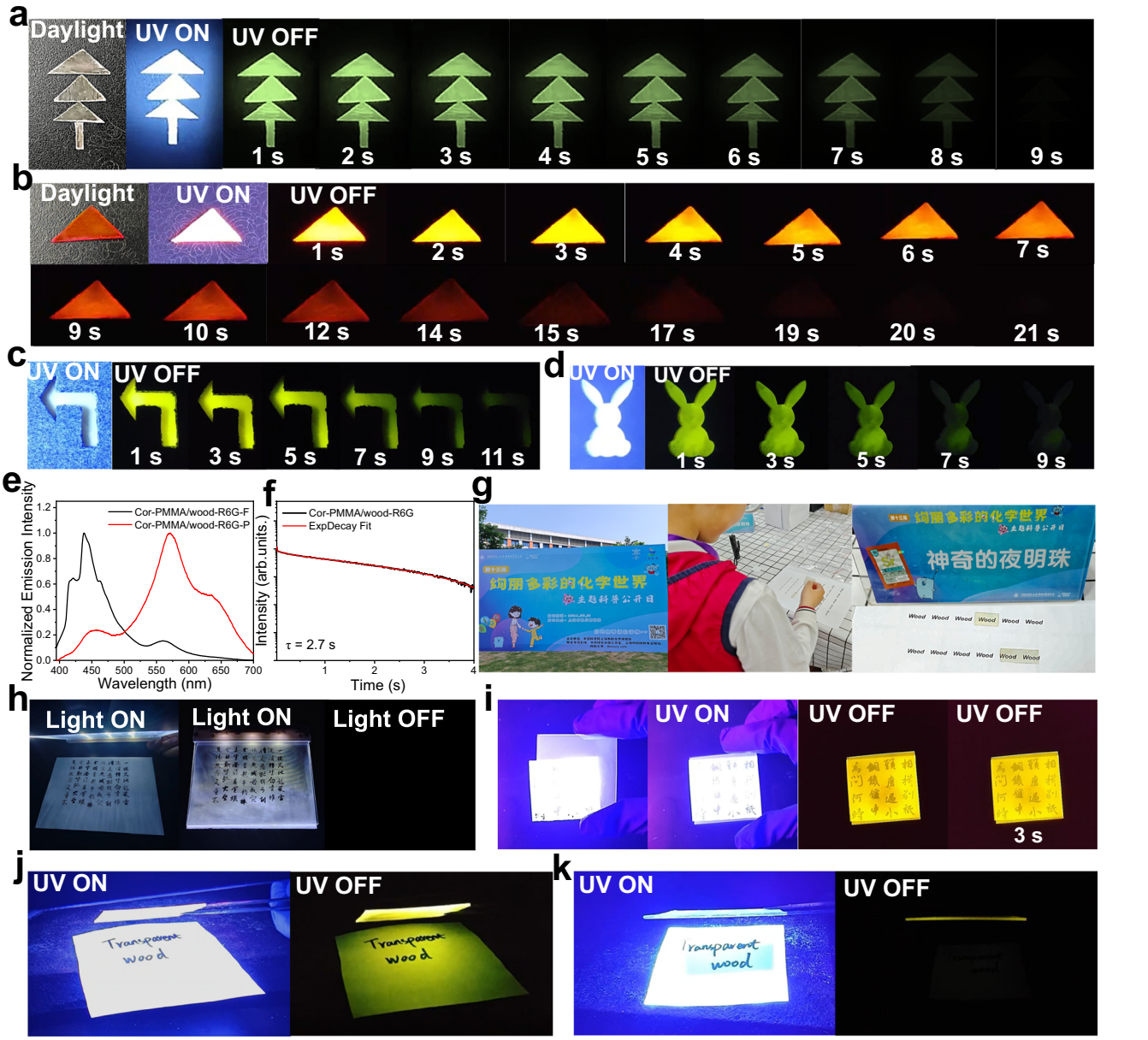

Fig. 8 | Function of RTP transparent wood. a Photographs of the plant-shaped assembly afterglow objects of **23F**-PMMA/wood materials; (**b**) Photographs of Cor-PMMA/wood-R6G three-component materials; (**c**) Left turn pattern of Cor-PMMA/wood afterglow materials; (**d**) Rabbit patterns of **3F**-PMMA/wood afterglow materials; (**e**) Room temperature steady-state and delayed emission (1 ms delay) spectra of Cor-PMMA/wood-R6G sample; (**f**) Room temperature afterglow decay of Cor-PMMA/wood-R6G materials monitored at 571 nm; (**g**) Transparent wood was exhibited at the Public Science Popularization Day held by our research institute; (**h**) A commercial flat-panel night reading light and (**i**) a flat afterglow lamp based on RTP transparent wood on a text; (**j**) A transparent wood-based afterglow panel excited by UV lamp behind the panel and (**k**) an opaque woo-based afterglow panel excited by UV lamp behind the panel.

RTP transparent wood can be used as display such as directional indications and safety exits (Fig. 8c and Supplementary Fig. 35a). It is well-known that Night Pearl is beautiful and can be used as a decoration. The RTP afterglow transparent wood can be considered as a biomass-based organic Night Pearl. Cartoon patterns have been produced to show its esthetics function (Fig. 8d and Supplementary Fig. 35b, c). Moreover, in terms of personalized customization, a SIOC logo has been made of RTP transparent wood, where SIOC represents Shanghai Institute of Organic Chemistry (Supplementary Fig. 35d). Furthermore, our research institute held a Public Science Popularization Day event in May 2024 (Fig. 8g), and RTP transparent wood has also been used as a display item to stimulate the interest of primary and secondary school students. These proof-of-demonstration studies indicate the combination of transparent wood and room temperature afterglow has broad prospects. In the aspect of RTP materials, transparent wood matrices not only provide the advantages of sustainability but also provide transparent property for RTP emitters, which allow excellent penetration of excitation lights and emission lights for the emergence of bright afterglow for diverse applications.

Inspired by the popular flat-panel night reading lights of recent years—characterized by their slim, lightweight design, portability, localized illumination that doesn't disturb others, and energy saving (Fig. 8h)—we developed a flat afterglow lamp based on transparent wood (Fig. 8i). In dark environments, this transparent wood-based afterglow panel can be placed close to text or images of interest, allowing the viewer to see the illuminated content through the panel, a feature that opaque afterglow panels cannot achieve. Additionally, for afterglow panels intended as both energy-efficient and esthetically

pleasing lighting, the excitation light source is generally positioned behind the panel. When transparent wood-based afterglow panels are excited from behind, the front surface can serve as a light source (Fig. 8j). In contrast, opaque afterglow panels emit only faint afterglow from the front after excitation, limiting their functionality for practical illumination (Fig. 8k).

Similar to other related materials, the RTP transparent wood is prone to contamination during use. The surface of most of the reported transparent wood has good or moderate hydrophobicity. Supplementary Table 4 summarizes mechanical strength and water contact angle of the reported transparent wood and other related biomass-based materials. Long-alkyl-chain-containing silane has been reported to modify the surface of transparent wood to enhance its hydrophobicity[13,106], which can resist the contamination of sewage but still cannot resist oil or fingerprint. Here we add KY-1203 (a kind of UV-curable perfluoropolyether-containing compounds that also allow thermal initiation polymerization, Shin-Etsu Chemical Co. Ltd.) during the preparation process of transparent wood to endow the materials with anti-smudge property (Fig. 9). The KY-1203 modified DCor-PMMA/wood afterglow materials not only exhibit bright RTP afterglow but also display anti-sewage property (Fig. 9a and Supplementary Fig. 36). The **23F**-PMMA/wood (without KY-1203) can be easily contaminated by fingerprints (with oil sludge) (Fig. 9b). In contrast, the KY-1203 modified **23F**-PMMA/wood RTP materials exhibit fingerprint removability (Fig. 9c, d). The surface of KY-1203 modified Cor-PMMA/wood shows water and oil repellency (a water contact angle of 108° and oleic acid contact angle of 78°) (Fig. 9e–h), which have been rarely reported in the literature of such type of materials. The anti-smudge function of RTP transparent wood would enrich their application scenarios.

Discussion

We report a preparation method for organic afterglow transparent wood using a thermal initiated polymerization and dopant-matrix design strategy. By using luminescent dopants, monomers, natural wood, and initiators, BF_2bdk-PMMA/wood afterglow materials are directly generated through thermal initiated polymerization. The polymer matrix enhances the intersystem crossing of BF_2bdk excited states through dipole-dipole interactions with BF_2bdk. The polymer matrix also provides a rigid environment for the BF_2bdk triplet to suppress its non-radiative decay and oxygen quenching. A comparison with other reported luminescent materials in terms of their afterglow characteristics, mechanical properties, and potential applications has been made in Supplementary Table 5 (the reported polymer-based and biomass-based afterglow materials that didn't measure mechanical property have not been included in this table). From Supplementary Table 5, one can find that the DCor-PMMA/wood materials in the present study exhibit the longest RTP lifetimes among the reported studies of such kind of afterglow materials. In addition, the KY-1203 fluorinated dopant-PMMA/wood RTP materials, which exhibit water/oil repellency and fingerprint removability, have been rarely reported in the literature. Moreover, the application of the dopant-PMMA/wood RTP materials in science popularization and other fields has also been explored. The RTP afterglow transparent wood we prepared has potential applications in mechanical properties, hydrophobicity, large-scale applications, as well as anti-counterfeiting materials or photonic devices.

We estimate the cost per ton of dopant-PMMA/wood RTP materials, detailed in Supplementary Table 6. BF_2bdk-PMMA/wood and Cor-PMMA/wood can be prepared at cost of ¥0.023 ($0.0032) and ¥0.027 ($0.0037) per gram, respectively. The cost of dopant-PMMA/wood RTP materials is higher than traditional building materials such as glass (0.0010 ~ 0.0015 ¥/g) and stone (0.0010 ~ 0.0030 ¥/g), slight higher than PMMA (0.018 ~ 0.020 ¥/g), but much lower than most of other RTP materials (please find the cost of biomass-based RTP materials in the published review article)[107]. If the RTP transparent wood is solely used as structural material, the RTP transparent wood is indeed significantly more expensive than conventional wood. Besides its mechanical property, the RTP transparent wood in the present study has excellent afterglow property and shows promising application in display and lighting, esthetics, personalized customization, and science popularization. These features increase the value of RTP transparent wood. During the purchasing process, many consumers prioritize cost-effectiveness rather than focusing solely on price. According to cost analysis in Supplementary Table 6 and literature reports, the cost-effectiveness of our RTP transparent wood is higher than that of other biomass-based RTP materials[107].

Methods

Physical measurements and instrumentation

Nuclear magnetic resonance (NMR) spectra were recorded on a JEOL Fourier-transform NMR spectrometer (400 MHz), including ^{1}H NMR,

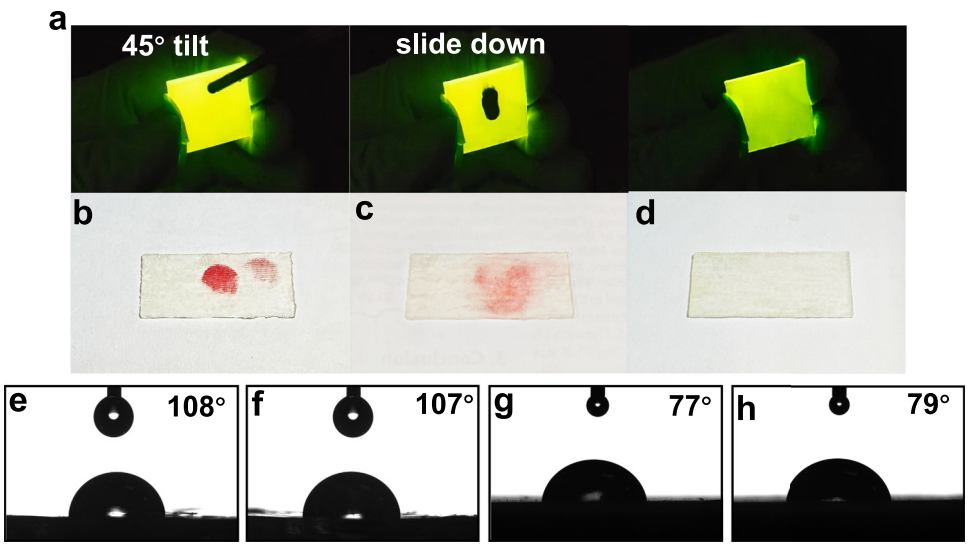

Fig. 9 | KY–1203 modified RTP transparent wood with anti-smudge property. **a** Photographs of KY–1203 modified DCor-PMMA/wood afterglow materials exhibiting the capability of repelling sewage (water droplets with black ink was used to mimic sewage); (**b**) Photographs of **23F**-PMMA/wood after being contaminated by fingerprints (with oil sludge); (**c**) Photographs of KY–1203 modified **23F**-PMMA/wood after being contaminated by fingerprints (with oil sludge) and (**d**) after cleaning up by wiping; (**e**) Water contact angle of KY–1203 modified **23F**-PMMA/wood and (**f**) KY–1203 modified Cor-PMMA/wood; (**g**) Oleic acid contact angle of KY-1203 modified **23F**-PMMA/wood and **h** KY-1203 modified Cor-PMMA/wood.

^{13}C NMR, and ^{19}F NMR. UV-Vis absorption spectra were recorded on a Techcomp UV1050 and Shimadzu UV-3600 spectrophotometer. The steady-state and delayed emission spectra were collected by Hitachi FL-4700 fluorescence spectrometer equipped with chopping systems; the delayed emission spectra were obtained with a delay time of ~1 ms. The excited state decay profiles in millisecond to second region were collected by Hitachi FL-4700 fluorescence spectrometer equipped with chopping systems. The fluorescence decay profiles in nanosecond region were recorded by using time-correlated single photon counting technique (TCSPC) on an Edinburgh FLS1000 fluorescence spectrometer equipped with a picosecond pulsed diode laser. Photoluminescence quantum yield was measured by a Hamamatsu absolute PL quantum yield measurement system based on a standard protocol. Photographs and videos were captured by HUAWEI P40 cameras. Before the capture, samples were irradiated by a 365 nm UV lamp (5 W) for ~5 s at a distance of ~15 cm. The morphologies of the wood were observed using the scanning electron microscopy (SEM) instrument of ZEISS Sigma 300 from Germany with a gold spraying process. Transmission electron microscopy (TEM) is used to observe the microstructure of wood by JEOL JEM-F200 from Japan. X-Ray Diffraction (XRD) is used to characterize the crystalline properties of wood by Rigaku SmartLab SE from Japan. The Fourier transform infrared (FT-IR) spectroscopy technique was also used for analysis. The FT-IR profiles were recorded on a Nicolet iS10 system with the scanning range of 4000-600 cm^{-1} and the resolution is 4.00 cm^{-1}. Thermogravimetric analysis (TGA) was performed to study thermal stability using 209 F3 Tarsus of Germany. Water contact angles were measured using a contact angle measuring instrument (OCA100, Data physics, Germany). The mechanical performance of the materials was tested using the universal testing machine (S2080, Instron, USA). MOE and tensile forces were also studied based on the GB/T 1928-2009 (General Requirements for Physical and Mechanical Tests of Wood) guidelines. The wood physical and mechanical test methods follow general rules, including ISO 3129 (1975, Wood-Sampling Methods and General Requirements for Physical and Mechanical Testing of Small Clear Wood Specimens), which specifies wood sampling methods and general requirements for physical and mechanical tests. These standards are considered the equivalent national standard (NEQ). The water absorption thickness expansion rate of transparent wood was tested according to the national standard (GB/T 15036-2018).

Synthesis of luminescent compounds via cascade reaction

Into a round bottom flask were added 5′-bromo-1,1′:3′,1″-terphenyl (309.2 mg, 1.0 mmol), 2,3-difluoro-4-methoxyphenylboronic acid (257.4 mg, 1.3 mmol), K_2CO_3 (138.4 mg, 1.0 mmol), $Pd(OAc)_2$ (11.1 mg, 0.05 mmol), ethanol (5 mL) and deionized water (2 mL). The reaction mixture was heated to 85 °C for 12 h. Then, the reaction mixture was diluted by dichloromethane, and K_2CO_3 precipitates were removed by suction filtration. The obtained crude product was condensed by rotary evaporation, and then purified by column chromatography over silica gel using petroleum ether/dichloromethane (1:3) as eluent to give colorless transparent oil. The colorless transparent oil was then added to a round bottom flask containing acetic anhydride (2.0 mL) and boron trifluoride diethyl etherate (0.9 mL). The reaction mixture was heated to 85 °C for 6 h and cooled to room temperature. The reaction mixture was extracted with dichloromethane and washed with deionized water. The crude product was dried on anhydrous magnesium sulfate, concentrated by rotary evaporation. The crude product purified by column chromatography over silica gel using petroleum ether/dichloromethane (2:3) to give pale yellow **23 F**. **23 F** was further purified by three cycles of recrystallization in spectroscopic grade dichloromethane/hexane. ^{1}H NMR (400 MHz, chloroform-d, relative to Me_4Si/ppm) δ 8.17, 8.15, 7.83, 7.81, 7.76, 7.72, 7.67, 7.66, 7.50, 7.49, 7.47, 7.43, 7.41, 7.39, 7.25, 7.22, 7.20, 6.88, 6.85, 6.83, 6.61, 3.96, 2.44. ^{13}C NMR (125 MHz, chloroform-d) δ 192.33, 147.88, 142.70, 140.39, 130.16, 129.73, 129.01, 128.16, 127.96, 127.36, 126.67, 125.58, 123.81, 108.44, 97.43, 56.74, 24.84. ^{19}F NMR (376 MHz, chloroform-d, 298 K) δ -125.51, -128.02, -145.57. HRMS m/z found (calcd for $C_{29}H_{21}O_3BF_4K^+$): 543.1172 (543.1177). The full details for the synthesis of compound **3 F** and its structural characterization results are available in the Supplementary Information.

Wood delignification

The chromophore groups in lignin can absorb visible lights and reduce light transmittance of the sample. The delignified process, which can remove the chromophore groups, is applied for the preparation of transparent wood, like Berglund's study[6] and many other reported studies. Balsa wood (*Ochroma lagopus*, moisture content, 5.42%, purchased from Yidimei franchise store, Hangzhou, China) was delignified by using 2 wt % $NaClO_2$ in CH_3COOH (pH = 4.6) at 80 °C. The reaction lasted for about 4 h until the wood became totally white. Bleach the delignified wood in H_2O_2 (30%) solution at 90 °C for 1 h. The treated samples were washed with ultrapure water to remove the chemical residue. Then, delignified balsa wood chips were stored in ethanol and acetone solvents to maintain the rigidity of its cellulose skeleton. In this study, transparent wood with different sizes and thicknesses of 0.5 mm, 1 mm, 2 mm, and 3 mm have been prepared; the size and thickness of transparent wood have been given in the main text and figure captions. It is known that the delignification process would be influenced by the thickness and size of wood[6]. Here we apply the frequently used conditions for wood delignification and find that most of the lignin can be removed.

Measurement of wood compositions

The compositions of wood were measured according to Van Soest method[108] on a ANKOM 220 fiber analyzer. The detailed experimental procedures have been added in the Supplementary Information. The compositions of raw wood, bleached wood (obtained by Hu's H_2O_2/UV method[1]), delignified wood (obtained by $NaClO_2$ treatment), and the delignified plus bleached wood (obtained by $NaClO_2$ treatment, followed by H_2O_2 soaking) have been measured to be 59.89% cellulose + 26.53% hemicellulose + 11.88% lignin, 58.26% cellulose + 25.15% hemicellulose + 10.01% lignin, 64.80% cellulose + 20.03% hemicellulose + 1.08% lignin, and 67.43% cellulose + 20.31% hemicellulose + 1.05% lignin, respectively (the raw data has been attached in Supplementary Information); in the literature, it has been reported that during the ADL (acid detergent lignin) step of the Van Soest method, a part of lignin would undergo degradation in 72% sulfuric acid, leading to the underestimation of lignin composition and consequently the overestimation of cellulose composition[109]. The data of wood compositions indicates that most of the lignin in balsa wood can be effectively removed through $NaClO_2$ treatment, and meanwhile some hemicellulose is also removed, aligning with findings reported in the literature[110]. In contrast, the bleached wood (obtained by Hu's H_2O_2/UV method) shows minimal changes or slight decreases in the contents of cellulose, hemicellulose, and lignin. Notably, in the bleached wood (obtained by Hu's H_2O_2/UV method), there is a slight reduction in lignin content, which may be attributed to the degradation of chromophores within the lignin, aligning with the UV-vis results of bleached wood (Supplementary Fig. 24, collected by an integrating sphere system).

Preparation of RTP afterglow transparent wood

To obtain RTP afterglow transparent wood, the filling materials were used to fill the delignified wood. 10 mL MMA doped with 0.3 wt% thermal initiator 2,2′-azobis(2-methylpropionitrile) (AIBN) was firstly pre-polymerized at 70 °C and then mixed with 0.3 wt% **3 F** or **23 F** by stirring under ultrasound until completely dissolved. Next, the dried delignified wood was immersed in the MMA mixture prepolymer solution and then placed in a vacuum drying oven, where the mixture

solution was filled into the delignified wood. Finally, the delignified wood filled with MMA mixture solution was assembled between two glass substrates. It was then wrapped in tin foil, placed in an oven, and polymerized at 70 °C for 4 h, leading to RTP afterglow transparent wood. PMMA-based RTP afterglow materials were prepared by directly mixing MMA solution with AIBN and adding **3 F** or **23 F** compounds. When preparing anti-smudge transparent wood, KY-1203 was first mixed with MMA at KY-1203/MMA volume ratio of 1/25, and then the other preparation steps are the same as above.

Data availability

The data that support the findings of this study are available in the article, supplementary information file, source data file or from the corresponding authors upon request. Source data are provided with this manuscript. The atomic coordinates of the optimized ground states of **3 F** and **23 F** are provided in Supplementary Data 1. Source data are provided with this paper.

References

1. Xia, Q. et al. Solar-assisted fabrication of large-scale, patternable transparent wood. *Sci. Adv.* **7**, eabd7342 (2021).
2. Zhu, M. et al. Highly anisotropic, highly transparent wood composites. *Adv. Mater.* **28**, 5181–5187 (2016).
3. Wu, X. et al. Transparent wood with self-cleaning properties for next-generation smart photovoltaic panels. *Appl. Surf. Sci.* **613**, 155927 (2023).
4. Fu, Q., Chen, Y. & Sorieul, M. Wood-based flexible electronics. *ACS Nano* **14**, 3528–3538 (2020).
5. Li, T. et al. A radiative cooling structural material. *Science* **364**, 760–763 (2019).
6. Li, Y. et al. Optically transparent wood from a nanoporous cellulosic template: combining functional and structural performance. *Biomacromolecules* **17**, 1358–1364 (2016).
7. Yang, H., Wang, H., Cai, T., Ge-Zhang, S. & Mu, H. Light and wood: a review of optically transparent wood for architectural applications. *Ind. Crop. Prod.* **204**, 117287 (2023).
8. Shi, R. et al. Preparation of sustainable transparent wood with glucose and phenol derived resin. *Ind. Crop. Prod.* **193**, 116234 (2023).
9. Li, Y. et al. Luminescent transparent wood. *Adv. Opt. Mater.* **5**, 1600834 (2017).
10. Wang, Z. et al. Preparation and performance of fluorescent transparent bamboo. *Ind. Crop. Prod.* **186**, 115222 (2022).
11. Zhang, T. et al. Constructing a novel electroluminescent device with high-temperature and high-humidity fesistance based on a flexible transparent wood film. *ACS Appl. Mater. Interfaces* **11**, 36010–36019 (2019).
12. Gan, J. et al. Wood-cellulose photoluminescence material based on carbon quantum dot for light conversion. *Carbohyd. Polym.* **290**, 119429 (2022).
13. Liu, S. et al. Self-densified optically transparent VO_2 thermochromic wood film for smart Windows. *ACS Appl. Mater. Interfaces* **13**, 22495–22504 (2021).
14. Mi, R. et al. Scalable aesthetic transparent wood for energy efficient buildings. *Nat. Commun.* **11**, 3836 (2020).
15. Montanari, C., Li, Y., Chen, H., Yan, M. & Berglund, L. A. Transparent wood for thermal energy storage and reversible optical transmittance. *ACS Appl. Mater. Interfaces* **11**, 20465–20472 (2019).
16. Samanta, A. et al. Reversible dual-stimuli-responsive chromic transparent wood biocomposites for smart window applications. *ACS Appl. Mater. Interfaces* **13**, 3270–3277 (2021).
17. Xia, R. et al. Transparent wood with phase change heat storage as novel green energy storage composites for building energy conservation. *J. Clean. Prod.* **296**, 126598 (2021).
18. Li, Y. et al. Optically transparent wood substrate for perovskite solar cells. *ACS Sustain. Chem. Eng.* **7**, 6061–6067 (2019).
19. Zhu, M. et al. Transparent and haze wood composites for highly efficient broadband light management in solar cells. *Nano Energy* **26**, 332–339 (2016).
20. Gan, J. et al. Full-wood utilization strategy toward a directional luminescent solar concentrator. *ACS Nano* **17**, 23512–23523 (2023).
21. Liu, L. et al. Switchable photochromic transparent wood as smart packaging materials. *Ind. Crop. Prod.* **184**, 115050 (2022).
22. Qiu, Z. et al. Transparent wood bearing a shielding effect to infrared heat and ultraviolet via incorporation of modified antimony-doped tin oxide nanoparticles. *Compos. Sci. Technol.* **172**, 43–48 (2019).
23. Van Hai, L. et al. Fabrication of eco-friendly transparent wood for UV-shielding functionality. *Ind. Crop. Prod.* **201**, 116918 (2023).
24. Yam, V. W.-W., Au, V. K.-M. & Leung, S. Y.-L. Light-emitting self-assembled materials based on d^8 and d^{10} transition metal complexes. *Chem. Rev.* **115**, 7589–7728 (2015).
25. Zhang, K. et al. Long-lived emissive probes for time-resolved photoluminescence bioimaging and biosensing. *Chem. Rev.* **118**, 1770–1839 (2018).
26. Uoyama, H., Goushi, K., Shizu, K., Nomura, H. & Adachi, C. Highly efficient organic light-emitting diodes from delayed fluorescence. *Nature* **492**, 234–238 (2012).
27. Xu, S. et al. Design of highly efficient deep-blue organic afterglow through guest sensitization and matrices rigidification. *Nat. Commun.* **11**, 4802 (2020).
28. Kuila, S., Garain, S., Bandi, S. & George, S. J. All-organic, temporally pure white afterglow in amorphous films using complementary blue and greenish-yellow ultralong room temperature phosphors. *Adv. Funct. Mater.* **30**, 2003693 (2020).
29. Yang, S. et al. Highly efficient organic afterglow from a 2D layered lead-free metal halide in both crystals and thin films under an air atmosphere. *ACS Appl. Mater. Interfaces* **12**, 1419–1426 (2020).
30. Guan, Z. et al. Multi-color pure organic room temperature phosphorescent materials with long lifetime and high efficiency. *Adv. Funct. Mater.* **34**, 2310198 (2023).
31. Ma, X., Wang, J. & Tian, H. Assembling-induced emission: an efficient approach for amorphous metal-free organic emitting materials with room-temperature phosphorescence. *Acc. Chem. Res.* **52**, 738–748 (2019).
32. Kenry, C. C. & Liu, B. Enhancing the performance of pure organic room-temperature phosphorescent luminophores. *Nat. Commun.* **10**, 2111 (2019).
33. Zhao, W., He, Z. & Tang, B. Z. Room-temperature phosphorescence from organic aggregates. *Nat. Rev. Mater.* **5**, 869–885 (2020).
34. Yan, X. et al. Recent advances on host–guest material systems toward organic room temperature phosphorescence. *Small* **18**, 2104073 (2022).
35. Zhang, G. et al. Multi-emissive difluoroboron dibenzoylmethane polylactide exhibiting intense fluorescence and oxygen-sensitive room-temperature phosphorescence. *J. Am. Chem. Soc.* **129**, 8942–8943 (2007).
36. Wu, B., Xu, X., Tang, Y., Han, X. & Wang, G. Multifunctional optical polymeric films with photochromic, fluorescent, and ultra-long room temperature phosphorescent properties. *Adv. Opt. Mater.* **9**, 2101266 (2021).
37. Zhai, Y. et al. Room temperature phosphorescence from natural wood activated by external chloride anion treatment. *Nat. Commun.* **14**, 2614 (2023).
38. Wan, K. et al. Structural materials with afterglow room temperature phosphorescence activated by lignin oxidation. *Nat. Commun.* **13**, 5508 (2022).

39. Yuan, J. et al. Sustainable afterglow materials from lignin inspired by wood phosphorescence. *Cell Rep. Phys. Sci.* **2**, 100542 (2021).
40. Liu, R. et al. Producing a room temperature phosphorescent film from natural wood using a top-down approach. *Adv. Funct. Mater.* **34**, 2312254 (2024).
41. Liu, Y. et al. Luminescent transparent wood based on lignin-derived carbon dots as a building material for dual-channel, real-time, and visual detection of formaldehyde gas. *ACS Appl. Mater. Interfaces* **12**, 36628–36638 (2020).
42. Zhou, B. et al. Highly efficient room-temperature organic afterglow achieved by collaboration of luminescent dimeric TADF dopants and rigid matrices. *J. Mater. Chem. C* **9**, 3939–3947 (2021).
43. Zhang, Y. et al. Large-area, flexible, transparent, and long-lived polymer-based phosphorescence films. *J. Am. Chem. Soc.* **143**, 13675–13685 (2021).
44. Li, Q. & Li, Z. Molecular packing: another key point for the performance of organic and polymeric optoelectronic materials. *Acc. Chem. Res.* **53**, 962–973 (2020).
45. Guo, S. et al. Recent progress in pure organic room temperature phosphorescence of small molecular host–guest systems. *ACS Mater. Lett.* **3**, 379–397 (2021).
46. Li, W. et al. Organic long-persistent luminescence from a thermally activated delayed fluorescence compound. *Adv. Mater.* **32**, 2003911 (2020).
47. Wang, J., Huang, Z., Ma, X. & Tian, H. Visible-light-excited room-temperature phosphorescence in water by cucurbit[8]uril-mediated supramolecular assembly. *Angew. Chem. Int. Ed.* **59**, 9928–9933 (2020).
48. Zhang, Z., Chen, Y. & Liu, Y. Efficient room-temperature phosphorescence of a solid-state supramolecule enhanced by cucurbit[6]uril. *Angew. Chem. Int. Ed.* **58**, 6028–6032 (2019).
49. Bian, L. et al. Simultaneously enhancing efficiency and lifetime of ultralong organic phosphorescence materials by molecular self-assembly. *J. Am. Chem. Soc.* **140**, 10734–10739 (2018).
50. Wang, G., Chen, X., Li, X., Zeng, Y. & Zhang, K. Mechanism landscape in pyrylium induced organic afterglow systems. *Chem. Sci.* **14**, 8180–8186 (2023).
51. Sun, Y. et al. Manipulation of triplet excited states for long-lived and efficient organic afterglow. *Adv. Opt. Mater.* **10**, 2101909 (2021).
52. Wang, X. et al. TADF-type organic afterglow. *Angew. Chem. Int. Ed.* **60**, 17138–17147 (2021).
53. Wang, G. et al. Two-component design strategy: TADF-Type organic afterglow for time-gated chemodosimeters. *Chem. Eng. J.* **431**, 134197 (2022).
54. Wang, X. et al. Merging thermally activated delayed fluorescence and two-photon ionization mechanisms for highly efficient and ultralong-lived organic afterglow. *Chem. Eng. J.* **460**, 141916 (2023).
55. Li, J. et al. A direct observation of up-converted room-temperature phosphorescence in an anti-Kasha dopant-matrix system. *Nat. Commun.* **14**, 1987 (2023).
56. Sun, Y., Wang, G., Li, X., Zhou, B. & Zhang, K. Achieving high afterglow brightness in organic dopant-matrix systems. *Adv. Opt. Mater.* **9**, 2100353 (2021).
57. Chen, X. et al. Difluoroboron β-diketonate systems: large transformation of photophysical mechanism induced by tiny structural modification or isomerization. *Adv. Opt. Mater.* **12**, 2301619 (2023).
58. Kabe, R. & Adachi, C. Organic long persistent luminescence. *Nature* **550**, 384–387 (2017).
59. Jinnai, K., Kabe, R., Lin, Z. & Adachi, C. Organic long-persistent luminescence stimulated by visible light in p-type systems based on organic photoredox catalyst dopants. *Nat. Mater.* **21**, 338–344 (2022).
60. Zhang, G., Palmer, G. M., Dewhirst, M. W. & Fraser, C. L. A dual-emissive-materials design concept enables tumour hypoxia imaging. *Nat. Mater.* **8**, 747–751 (2009).
61. Wang, X. et al. Pure organic room temperature phosphorescence from excited dimers in self-assembled nanoparticles under visible and near-infrared irradiation in water. *J. Am. Chem. Soc.* **141**, 5045–5050 (2019).
62. Dang, Q. et al. Room-temperature phosphorescence resonance energy transfer for construction of near-infrared afterglow imaging agents. *Adv. Mater.* **32**, 2006752 (2020).
63. Wang, Y. et al. High performance of simple organic phosphorescence host–guest materials and their application in time-resolved bioimaging. *Adv. Mater.* **33**, 2007811 (2021).
64. Yu, Y. et al. Room-temperature-phosphorescence-based dissolved oxygen detection by core-shell polymer nanoparticles containing metal-free organic phosphors. *Angew. Chem. Int. Ed* **56**, 16207–16211 (2017).
65. Liu, J. et al. Organic afterglow emulsions exhibiting 2.4 s phosphorescence lifetimes and specific protein binding property. *Adv. Opt. Mater.* **10**, 2201502 (2022).
66. Gan, N., Shi, H., An, Z. & Huang, W. Recent advances in polymer-based metal-free room-temperature phosphorescent materials. *Adv. Funct. Mater.* **28**, 1802657 (2018).
67. Gao, H. & Ma, X. Recent progress on pure organic room temperature phosphorescent polymers. *Aggregate* **2**, e38 (2021).
68. Hirata, S. Recent advances in materials with room-temperature phosphorescence: photophysics for triplet exciton stabilization. *Adv. Opt. Mater.* **5**, 1700116 (2017).
69. Singh, M. et al. Recent advances of cocrystals with room temperature phosphorescence. *Adv. Opt. Mater.* **9**, 2002197 (2021).
70. Jinnai, K., Kabe, R. & Adachi, C. Long-persistent luminescence: wide-range tuning and enhancement of organic long-persistent luminescence using emitter dopants. *Adv. Mater.* **30**, 1870286 (2018).
71. Huang, J. et al. Polymer-based TADF-type organic afterglow. *J. Phys. Chem. C* **126**, 20728–20738 (2022).
72. Lü, Z. et al. Colorful room-temperature phosphorescence including white afterglow from mechanical robust transparent wood for time delay lighting. *Small Struct.* **5**, 2300567 (2024).
73. Wang, L., Liu, Y., Zhan, X., Luo, D. & Sun, X. Photochromic transparent wood for photo-switchable smart window applications. *J. Mater. Chem. C* **7**, 8649–8654 (2019).
74. Gmelch, M., Achenbach, T., Tomkeviciene, A. & Reineke, S. High-speed and continuous-wave programmable luminescent tags based on exclusive room temperature phosphorescence (RTP). *Adv. Sci.* **8**, 2102104 (2021).
75. Gmelch, M., Thomas, H., Fries, F. & Reineke, S. Programmable transparent organic luminescent tags. *Sci. Adv.* **5**, eaau7310 (2019).
76. Yao, X. et al. Room-temperature phosphorescence enabled through nacre-mimetic nanocomposite design. *Adv. Mater.* **33**, 2005973 (2021).
77. Louis, M. et al. Blue-light-absorbing thin films showing ultralong room-temperature phosphorescence. *Adv. Mater.* **31**, 1807887 (2019).
78. Su, Y. et al. Excitation-dependent long-life luminescent polymeric systems under ambient conditions. *Angew. Chem. Int. Ed.* **59**, 9967–9971 (2020).
79. Wu, H. et al. Tailoring noncovalent interactions to activate persistent room-temperature phosphorescence from doped polyacrylonitrile films. *Adv. Funct. Mater.* **31**, 2101656 (2021).
80. Li, D. et al. Boosting organic afterglow performance via a two-component design strategy extracted from macromolecular self-assembly. *J. Phys. Chem. Lett.* **13**, 5030–5039 (2022).

81. Zhou, Y. et al. Sunlight-activated hour-long afterglow from transparent and flexible polymers. *Adv. Mater.* **36**, 2312439 (2024).
82. Chen, X. et al. Merging photoinitiated bulk polymerization and the dopant-matrix design strategy for polymer-based organic afterglow materials. *Polym. Chem.* **13**, 4641–4649 (2022).
83. Li, X. et al. Intense organic afterglow enabled by molecular engineering in dopant-matrix systems. *ACS Appl. Mater. Interfaces* **14**, 1587–1600 (2022).
84. Li, J. et al. Developing bright afterglow materials via manipulation of higher triplet excited states and relay synthesis in difluoroboron *β*-diketonate systems. *Adv. Opt. Mater.* **12**, 2302311 (2023).
85. Wang, J. et al. Organic composite crystal with persistent room-temperature luminescence above 650 nm by combining triplet–triplet energy transfer with thermally activated delayed fluorescence. *CCS Chem.* **2**, 1391–1398 (2020).
86. Kuila, S. & George, S. J. Phosphorescence energy transfer: ambient afterglow fluorescence from water-processable and purely organic dyes via delayed sensitization. *Angew. Chem. Int. Ed.* **59**, 9393–9397 (2020).
87. Lei, Y. et al. Wide-range color-tunable organic phosphorescence materials for printable and writable security inks. *Angew. Chem. Int. Ed* **59**, 16054–16060 (2020).
88. Hirata, S. et al. Efficient persistent room temperature phosphorescence in organic amorphous materials under ambient conditions. *Adv. Funct. Mater.* **23**, 3386–3397 (2013).
89. Chen, C. et al. Carbazole isomers induce ultralong organic phosphorescence. *Nat. Mater.* **20**, 175–180 (2021).
90. Kasha, M., Rawls, H. R. & El-Bayoumi, M. A. The exciton model in molecular spectroscopy. *Pure Appl. Chem* **11**, 371–392 (1965).
91. Chen, P. et al. Carbazole-containing difluoroboron β-diketonate dyes: two-photon excited fluorescence in solution and grinding-induced blue-shifted emission in the solid state. *J. Mater. Chem. C* **5**, 12538–12546 (2017).
92. Poon, C.-T., Lam, W. H., Wong, H.-L. & Yam, V. W.-W. Photochromic dithienylethene-containing triarylborane derivatives: facile approach to modulate photochromic properties with multi-addressable functions. *Chem. Eur. J.* **21**, 2182–2192 (2015).
93. Wang, S., Cai, J., Sadygov, R. & Lim, E. C. Intramolecular charge transfer and solvent-polarity dependence of radiative decay rate in photoexcited dinaphthylamines. *J. Phys. Chem.* **99**, 7416–7420 (1995).
94. Gillett, A. J. et al. Dielectric control of reverse intersystem crossing in thermally activated delayed fluorescence emitters. *Nat. Mater.* **21**, 1150–1157 (2022).
95. Samanta, A. et al. Charge regulated diffusion of silica nanoparticles into wood for flame retardant transparent wood. *Adv. Sustain. Syst.* **6**, 2100354 (2022).
96. Reza, M. et al. Transparent wood transmission electron microscopy for wood and fiber analysis- a review. *BioResources* **10**, 6230–6261 (2015).
97. Wang, J. et al. Moisture and oxygen barrier properties of cellulose nanomaterial-based films. *ACS Sustain. Chem. Eng.* **6**, 49–70 (2018).
98. Jiang, Y. et al. Hemicellulose-rich transparent wood: microstructure and macroscopic properties. *Carbohydr. Polym.* **296**, 119925 (2022).
99. Yu, Z. et al. Transparent wood containing Cs_xWO_3 nanoparticles for heat-shielding window applications. *J. Mater. Chem. A* **5**, 6019–6024 (2017).
100. Mieno, H., Kabe, R., Notsuka, N., Allendorf, M. D. & Adachi, C. Long-lived room-temperature phosphorescence of coronene in zeolitic imidazolate framework ZIF-8. *Adv. Opt. Mater.* **4**, 1015–1021 (2016).
101. Wu, M. et al. Two-component design strategy: achieving intense organic afterglow and diverse functions in coronene-matrix systems. *J. Phys. Chem. C* **125**, 26986–26998 (2021).
102. Zhai, X. et al. Anti-smudge organic afterglow panels. *Adv. Funct. Mater.* **34**, 2405637 (2024).
103. Yu, J. et al. Efficient visible-light-activated ultra-long room-temperature phosphorescence triggered by multi-esterification. *Angew. Chem. Int. Ed* **62**, e202316647 (2023).
104. Li, Y. et al. Optically transparent wood: recent progress, opportunities, and challenges. *Adv. Opt. Mater.* **6**, 1800059 (2019).
105. Ma, L. et al. A universal strategy for tunable persistent luminescent materials via radiative energy transfer. *Angew. Chem. Int. Ed.* **61**, e202115748 (2022).
106. Zhu, L. et al. Transparent bioplastics from super-low lignin wood with abundant hydrophobic cellulose crystals. *ACS Sustain. Chem. Eng.* **10**, 13775–13785 (2022).
107. Luo, X. et al. Room-temperature phosphorescent materials derived from natural resources. *Nat. Rev. Chem.* **7**, 800–812 (2023).
108. Van Soest, P. J., Robertson, J. B. & Lewis, B. A. Methods for dietary fiber, neutral detergent fiber, and nonstarch polysaccharides in relation to animal nutrition. *J. Dairy Sci.* **74**, 3583–3597 (1991).
109. Adjalle, K., Larose, L.-V., Bley, J. & Barnabé, S. The effect of organic nitrogenous compound content and different pretreatments on agricultural lignocellulosic biomass characterization methods. *Cellulose* **24**, 1395–1406 (2017).
110. Wang, Y., Yang, Y., Qu, Y. & Zhang, J. Selective removal of lignin with sodium chlorite to improve the quality and antioxidant activity of *xylo*-oligosaccharides from lignocellulosic biomass. *Bioresource Technol.* **337**, 125506 (2021).

Acknowledgements

We thank the financial supports from National Natural Science Foundation of China (No. 22475228 and 22175194 to K.Z.), Hundred Talents Program from Shanghai Institute of Organic Chemistry (No. Y121078 to K. Z.), Pioneer Hundred Talents Program of Chinese Academy of Sciences (No. E320021 to K. Z.), the Strategic Priority Research Program of the Chinese Academy of Sciences (No. XDB0610000 to K. Z.), and Ningbo Natural Science Foundation (No. 2023J243 to K.Z.).

Author contributions

X.P., X.C., G.W. and X.Z. performed the experimental studies and carried out the analysis. T.W. performed the computational studies. K.Z. supervised the work.

Competing interests

The authors declare no competing interests.

Additional information

Supplementary information The online version contains supplementary material available at https://doi.org/10.1038/s41467-025-55990-z.

Correspondence and requests for materials should be addressed to Kaka Zhang.

Peer review information *Nature Communications* thanks Yan Wu and the other, anonymous, reviewers for their contribution to the peer review of this work. A peer review file is available.